IEEE Access
Multidisciplinary | Rapid Review | Open Access Journal

Received 7 September 2022, accepted 14 September 2022, date of publication 20 September 2022,
date of current version 12 October 2022.

Digital Object Identifier 10.1109/ACCESS.2022.3208162

METHODS

Detection of AC Arc Faults of Aviation Cables Based on H-I-W Three-Dimensional Features and CNN-LSTM Neural Network

XIAOLIN LIU[1], DESHUN HUANG[1], TAO JING[1], AND YANAN ZHANG[2]
[1]College of Electronic Information and Automation, Civil Aviation University of China, Tianjin 300300, China
[2]AVIC Tianjin Aviation Electromechanical Company Ltd., Tianjin 300308, China

Corresponding author: Xiaolin Liu (caucyanjiusheng@163.com)

This work was supported in part by the Central University Fund of Tianjin under Grant 3122018D004; and in part by the Research on Fault Prediction and Health Management Technology Based on Remote Power Distribution Unit (RPDU) through the School Enterprise Cooperation Project of Aviation Industry Corporation of China, Ltd. (AVIC) Tianjin Electromechanical Company Ltd., under Gant 402203.

ABSTRACT Aiming at the difficulty in identifying subtle AC arcs in aviation cables, this paper proposes an arc fault detection method based on the combination of three-dimensional features and convolutional neural network-long short term memory (CNN-LSTM). Firstly, based on the SAE AS5692A standard, the vibration series test, cutting parallel test, and wet arc trajectory parallel test were respectively conducted and the arc current signals under four types of loads were collected to analyze the arc faults under different incentives. Then, the three-dimensional features of arc current including Hurst exponent, inter-harmonic variance, and wavelet energy entropy (H-I-W) were extracted with an improved algorithm so as to enhance the fault identification capability and overcome the limitation of single-dimensional feature detection. Finally, a grid search algorithm was used to find out the optimal parameters, and a three-dimensional reference input CNN-LSTM neural network was designed to detect arc faults. The experimental results showed that the average detection accuracy of the proposed method for the three AC arc faults respectively reached 98.52%, 99.23%, and 98.51%. The real-time performance of the proposed method was better than the comparison methods, proving the feasibility and effectiveness of the proposed method.

INDEX TERMS Aviation cable, AC arc fault, H-I-W three-dimensional feature, CNN-LSTM neural network.

I. INTRODUCTION

Aviation cables are the most important components in aircraft systems and mainly responsible for energy transmission and control signal transmission between avionics [1]. Compared with ordinary power cables, aviation cables are characterized by thinner insulation layers and the longer service period in humid environments with intense vibration, friction, and radiation. They are highly susceptible to cracks and breakage [2], [3], thus inducing AC arc faults. When an arc occurs, the temperature of the arc center can reach several thousand degrees [4] and cause cable combustion and fire in the aircraft, thus threatening flight safety. Due to the circuit load and environmental factors, the AC arc current has a small amplitude and hidden characteristics and is difficult to be detected with thermal circuit breakers (TCB) and solid-state power controller (SSPC) [5]. It is therefore necessary to develop arc fault detection methods for the purposes of improving the identification rate of AC arc faults in aviation cables and enhancing flight safety.

At present, AC arc fault detection methods are mainly divided into two categories. The first is the detection of physical phenomena such as arc lights or arc sounds generated by the occurrence of an arc fault. The ultraviolet range of 300 nm to 330 nm was used as the wavelength for arc fault detection and satisfactory detection results were achieved [6]. Yun *et al.* [7] collected the characteristic light of the arc with the collection system on the roof of the train, analyzed the

The associate editor coordinating the review of this manuscript and approving it for publication was Donato Impedovo.

arc spectral distribution, and determined the range of 275 nm to 285 nm as the detection characteristic waveband of the short-gap arc of the pantograph-catenary system. However, the determined detection band could identify only one type of arc faults. A loop antenna or sensor was designed to collect electromagnetic radiation and then arc fault detection was performed based on the extracted features (log spectral distance, pulse oscillation time, and characteristic frequency distribution) of the collected electromagnetic radiation signals [8], [9]. However, the physical feature extraction of arc signals requires numerous sensors and the installation positions of sensors affect the operation of the power distribution system of an aircraft. Moreover, the strong ambient noise and interference in flight may affect the output of sensors, so it is difficult to carry out accurate fault identification based on the physical characteristics of the arc.

The second category is the detection method based on the characteristic changes of voltage and current of the signals in the time domain, frequency domain, and time-frequency domain in the case of an arc. The time-domain features and parameters are computed rapidly and easily embedded in hardware devices such as arc fault circuit breakers (AFCB), so relevant time-domain arc detection algorithms have been proposed. Sultan *et al.* proposed arc fault detection based on current peaks [10]. Lezama *et al.* calculated current autocorrelation coefficients and obtained arc detection metrics through algebraic estimation of autocorrelation coefficients [11]. Metrics such as kurtosis, mean value, variance, and third, and fourth accumulation were also introduced into arc fault detection [12]. A method based on high-frequency pulse components of coupled signals was used in the identification of AC series arc faults in residential buildings [13], [14]. On the basis of this method, Run *et al.* proposed short observation window singular value decomposition and reconstruction algorithm [15] and time series reconstruction algorithm [16] for enhancing high-frequency pulse components and realized series arc fault identification. However, due to the low amplitude and weak characteristics of AC arc currents of aviation cables, it is difficult to accurately identify the arc faults with time-domain features alone. In some studies, it was found that the frequency domain information changed to some degree when an arc occurred. Guan *et al.* derived an expression for the signal power spectrum with the Welch algorithm for arc identification based on spectral changes [17]. When an arc fault occurred, some new high-frequency components of the circuit current appeared, so identification of arc faults based on high-frequency components was the main frequency domain method [18]. Lezama *et al.* [19] performed arc fault detection by comparing the low-frequency band of current, the high-frequency band of voltage, and the root means square value of current and voltage with the corresponding threshold values. When a certain number of consecutive occurrences of faults were detected, the occurrence of an arc fault was determined. However, various arc faults in aviation cables had different characteristics, so it was difficult to apply the arc fault detection method based on comparison results in aviation electrical systems. In the advanced harmonic study [20], the 3rd and 5th harmonics of the signal were used in arc fault detection. Li *et al.* used the half-cycle analysis method and fast Fourier transform (FFT) to detect arc faults [21]. Artale *et al.* used the chirp zeta transform (CZT) to analyze the low-frequency harmonic current in the case of an arc [22]. Karakose *et al.* proposed an arc detection method based on signal normalization and S-transform (ST) for arch network systems and applied fuzzy theory and ST in arc fault detection [23]. Chen *et al.* performed low-voltage series arc fault identification with empirical modal decomposition (EMD) and Hilbert's Huang transform (HHT) [24]. In time-frequency domain, Wavelet Transform (WT) is an effective tool to analyze time series. Through 550 sets of arc experiments, Qi *et al.* found that the selection of mother wavelet, number of decomposition layers, and sampling frequency greatly affected the arc fault detection performance [25]. Mortazavi *et al.* extracted the dynamic features of signals with smooth WT, input them into support vector machine (SVM) for arc identification, and improved the identification of arc faults from a few amperes to several hundred amperes [26], but it was difficult to achieve the same identification effect for low-current vibration arc faults.

To integrate the advantages of different features, Qu *et al.* extracted a large number of features and selected 4 time-domain features and 10 frequency-domain features for arc fault identification [4], but the fusion of too many features could lead to overfitting and accuracy reduction [27] and increase the embedding difficulty and the cost of the algorithm. Therefore, it is extremely important to select an appropriate number of effective signal features.

In recent years, intelligent learning methods have also been gradually introduced into arc detection research due to their excellent processing capability of complex signals. Wang *et al.* proposed to extract signal features with sparse matrix, and input them into fully connected neural network (FCNN) for residential AC arc identification [28]. Jiang *et al.* carried out series arc fault identification based on random forest (RF) and deep neural network (DNN) [29]. Amiri *et al.* proposed a method for series arc fault detection in photovoltaic systems based on voltage signal determinism and used a recursive graph method to derive the signal determinism for detecting series arc faults [30].Yu *et al.* proposed an arc fault detection method based on raw data and parallel deep neural networks (PDNN), and demonstrated that the detection accuracy and stability of PDNN were better than DNN [31]. Nevertheless, it would take a lot of time to train neural networks with raw data. Li *et al.* proposed a recurrent neural network (RNN) method for series arc fault detection in multi-load systems, and further improved the detection speed and accuracy through fast continuous monitoring and probability classification results [32]. Furthermore, Wang *et al.* proposed an arc recognition model based on current raw data and convolutional neural network (CNN), and implemented the model on Raspberry Pi 3B to achieve good results [33].

A time-domain visualization (TDV) method converted the time series into a two-dimensional image, which was then fed into a CNN [34], [35] or Long-Short Term Memory (LSTM) [36] neural network for arc fault detection, and the better identification results of AC series arcs in residences demonstrated the application of CNN and LSTM in arc fault detection. CNN is a typical network for complex fault diagnosis in deep learning methods and aims to convolve and pool the signal layer by layer through convolutional and pooling layers and extract the features of the input data layer by layer. As a kind of neural network, LSTM neural network can solve gradient disappearance and gradient explosion problems in the training process of long sequences and has the excellent processing ability and model parameter optimization capability for time series data. However, LSTM without the specialized feature mining function shows average results when dealing with the data with weak fault information [37]. Therefore, the idea of combining CNNs with LSTMs has been proposed in fault recognition research. Currently, CNN-LSTM neural networks are widely used in the fault detection of bearings [37] because the combination of CNN and LSTM for the analysis and processing of time series is more advantageous in complex environments.

Aiming at the problems of the hidden characteristics and the difficulty in accurate identification of arc faults in aviation cables, this paper proposes an AC arc fault detection method for aviation cables based on the combination of H-I-W three-dimensional features and CNN-LSTM neural networks. The method improved the arc fault identification through extracting features from three dimensions separately and combined the excellent weak feature extraction ability of CNN with the good fault identification ability of LSTM. The method proposed in this paper can achieve the efficient and accurate detection of AC arc faults in aviation cables.

The paper is organized as follows. In Section II, the arc simulation test schemes under different loads are presented and the circuit currents are acquired. In Section III, the arc fault detection strategy is described. In Section IV, three improved algorithms are designed to extract H-I-W three-dimensional features. In Section V, the CNN-LSTM arc detection model is designed to detect the normal status and arc fault. The method has high detection accuracy and reliability of AC arc faults in aviation cables.

II. ARC EXPERIMENTS AND DATA ACQUISITION

Aviation cables are applied in complex environments and it is difficult to simulate their actual arcing situation through traditional point contact tests. All the factors causing AC arc faults, including terminal vibration, cut-off, and water drop, are fully considered. Furthermore, under the same power supply voltage and load type, three typical tests (vibration test, cutting test, and wet arc trajectory arc test) were carried out to simulate the generation of arc in actual avionics system environments. In this way, the measured data of arc currents were similar to the actual data and provided a reliable basis for arc fault detection.

A. ARC SIMULATION EXPERIMENT

UL1699 is Standard for Safe Arc-Fault Circuit-Interrupters [38] and SAE AS5692A is the Standard for Arc Fault Test Platforms [39]. Based on arc fault circuit breaker standard UL1699 and aviation standard SAE AS5692A, vibration test, cutting test, and wet arc trajectory arc test were carried out. The arc test circuits are shown in Fig. 1 to Fig. 3.

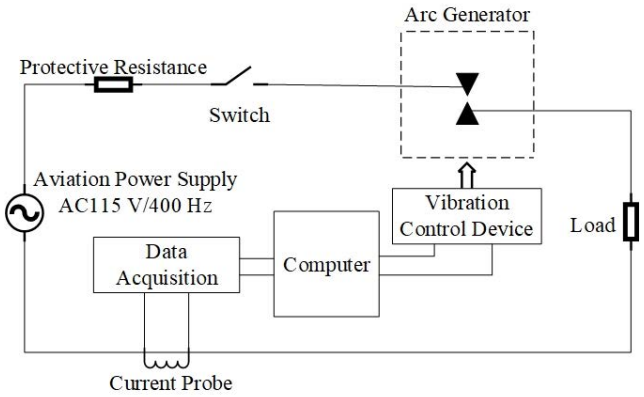

FIGURE 1. Vibration test circuit.

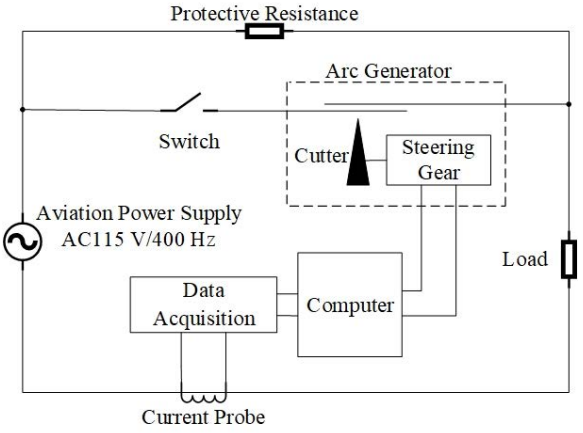

FIGURE 2. Cutting test circuit.

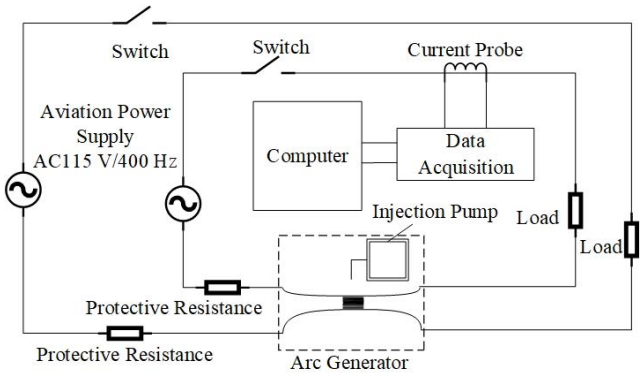

FIGURE 3. Wet arc trajectory test circuit.

In the vibration test, the test bench was continuously vibrated with the vibration control device, thus resulting in

intermittent contact at cable connection terminals and simulating arc faults caused by loose electrical connectors due to aircraft vibration. In the cutting test. a steering gear was used to move the cutter downward, thus simulating an arc fault caused by a short circuit between cables under the complex environmental stress. In the wet arc trajectory test, the injection pump was controlled to drop saline water with a concentration of 3±0.5% on the test cable at a rate of 8 drops per minute so as to simulate an arc fault caused by condensed water droplets at the breakage of different wire harnesses due to the changes in ambient temperature.

In the test, the power cabinet generated 115 V/400 Hz driving voltage and power current.

The current probe used was Tektronix TCP303 with a bandwidth of 0 Hz to 15 MHz and a minimum measurable current of 5 mA.

The data were acquired with Tektronix MDO 4034C with its analog bandwidth of 1 GHz and the maximum sampling rate of a single channel, 5 GS/s.

MIL-DTL-81381 cable was used in vibration tests and M27500-24WN2N24 cable was used in cutting test and wet arc track test.

Aviation cables were connected with lamp (resistive load), aviation solenoid (inductive load), seat (capacitive load), and the non-linear motor load. Therefore, two types of loads were used in the test: linear load and nonlinear load. In Table 1, Load 1, Load 2, and Load 3 are respectively pure resistive load, inductive load, and capacitive load. The nonlinear Load 4 is the rotating electrical machine (REM).

TABLE 1. H-I-W feature of wet arc trajectory test.

Linear			Nonlinear
Load 1	Load 2	Load 3	Load 4
20 Ω	20 Ω plus solenoid valve	20 Ω plus 47 μF	REM

B. ARC FAULT DATA ACQUISITION

The sampling frequency used in the arc study could be determined with the spectral band, in which the arc information is mainly distributed [26]. FFT operation was conducted on the arc signal. The signal spectrum is plotted in Fig. 4.

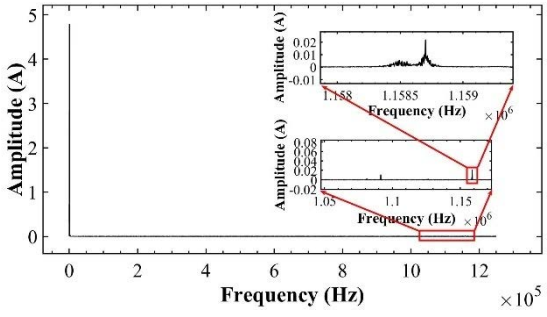

FIGURE 4. FFT waveform of test current.

The arc information of the signal was still detected around the frequency of 1.1587 MHz (Fig. 4). Therefore, for acquiring complete signal information, the sampling rate chosen in the test was 2.5 MHz. When the smallest observation window (OW) was selected, the main spectral information should be contained [14]. Different OWs (0.5 cycle, 1 cycle, and 2 cycles) were compared and the spectral information near the fundamental frequency was in the normal state (Fig. 5). At OW=0.5 cycle, the spectrum near the fundamental frequency was leaked severely. Compared to OW=2 cycles, OW=1 cycle could represent the spectral information of the signal completely. When an arc fault occurred, the waveforms of adjacent current cycles became different. Therefore, in order to accurately identify arc faults, we used 1 cycle of the current signal as one calculation unit for the feature extraction algorithm below.

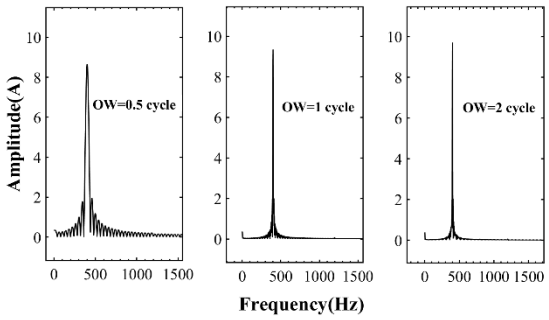

FIGURE 5. Spectral effects of different OWs on the signal in the normal state.

The arc fault test current was collected with a current probe and each test intercepted 30 cycle currents including normal and fault currents with 6250 sampling points per cycle. The test current signals collected under Load 1 are shown in Fig. 6.

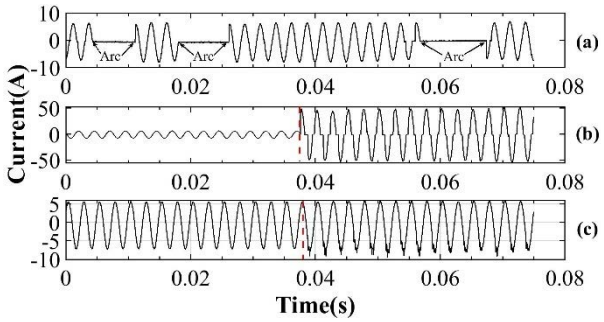

FIGURE 6. Arc test current waveforms under Load 1: (a) vibration test, (b) cutting test, and (c) wet arc trajectory test.

From the test phenomena and test current waveforms in Fig. 6, the conclusions can be drawn as follows:

Firstly, under a linear load, the current waveform was in a stable sine wave state before the arc fault occurred. When an arc fault occurred, the vibration test current decreased to a smaller value close to 0 and then maintained for a short period of time. The amplitude of the cutting test current instantly

increased tenfold and the wet arc track test current showed a slight burr at the trough.

Secondly, the arc current waveforms of the cutting test had an area where the current was close to zero before and after the zero-crossing point because of the damaged cable core and the arc extinguishing and re-igniting process before and after the current zero point.

Thirdly, during the arcing test, the arc in the vibration test was weak and had a short duration and the arc in the cutting test was intense and accompanied by sparks. The arc burning time in the wet arc trajectory test was synchronized with the time when saline water dropped at the damaged cable.

Fourthly, at the end of the arc test, black charcoal remained at the position where the arc occurred and the cutter in the cutting test showed an obvious corrosion nick.

The arc test current waveforms under Load 2, Load 3, and Load 4 are shown in Fig. 7.

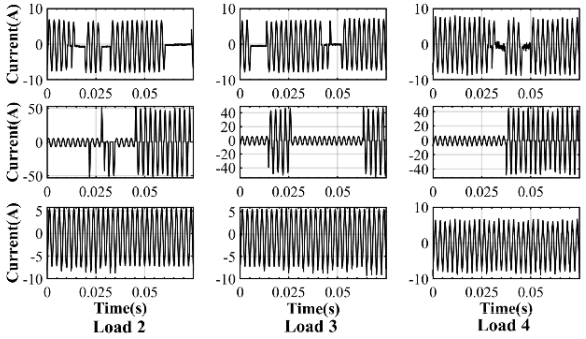

FIGURE 7. Arc test current waveforms under Load 2, Load 3, and Load 4: (a) vibration test, (b) cutting test, and (c) wet arc trajectory test.

From the analysis results of current waveforms shown in Fig. 7, it can be seen that the above conclusions are also applicable to resistive inductive load, resistive capacitive load, and rotating motor load. Under normal conditions, the test current was below 7 A, which was less than the maximum AFCI nominal value, 20 A. When an arc fault occurred, the currents in vibration tests and the wet arc track test were less than 20 A and the current in the cutting test was within 48.5 A and less than AFCI short-circuit current. Therefore, the current used in the test met the current detection requirements in UL1699 standard.

In practice, the cutting test arc rarely occurs. Once it occurred, it caused a serious fire. However, an arc fault was prone to occur in the vibration test and the wet arc trajectory test. The changes of the current after the occurrence of an arc are shown in Fig. 6 and Fig. 7. The arc current in the cutting test showed obvious changes. In the case of arc fault, the arc current in the vibration test became smaller and the increase of the arc current in the wet arc trajectory test was small. The above two arc currents could not meet circuit breaker action requirements of TCB and traditional SSPC.

III. ARC FAULT DETECTION STRATEGY

Based on the arc test platform, under four typical loads, three kinds of arc tests were carried out, respectively. After acquiring the current signals, we performed arc fault detection according to the scheme shown in Fig. 8.

The three arc faults were accompanied by unique current variations and the original data were huge and would lead to too long training time and low recognition rate of CNN-LSTM. Therefore, the H-I-W features were firstly extracted by using time domain, frequency domain, and energy entropy methods. In time domain, we introduced Hurst exponent as the time domain feature of the current signal. In order to obtain more arc fault information on the basis of frequency-domain harmonics, we calculated the inter-harmonic variance of the current signal as a frequency-domain feature. In order to realize the comprehensive detection of AC arc faults of aviation cables, we used the wavelet energy entropy as the energy entropy feature to achieve three-dimensional feature extraction. However, the extracted features were affected by load type, wire type, and fault point, so it was difficult to flexibly and effectively detect arc faults by setting the H-I-W determination threshold alone. In addition, different types of arc currents showed different trends, so it was impossible to apply a fixed detection threshold value in different kinds of arcs. Therefore, based on the advantages of CNN and LSTM neural network, we designed a CNN-LSTM hybrid network arc detection model with a simple structure and stable computational efficiency. The extracted three-dimensional features were then fed into the CNN-LSTM detection model so as to realize the intelligent detection of AC arc faults.

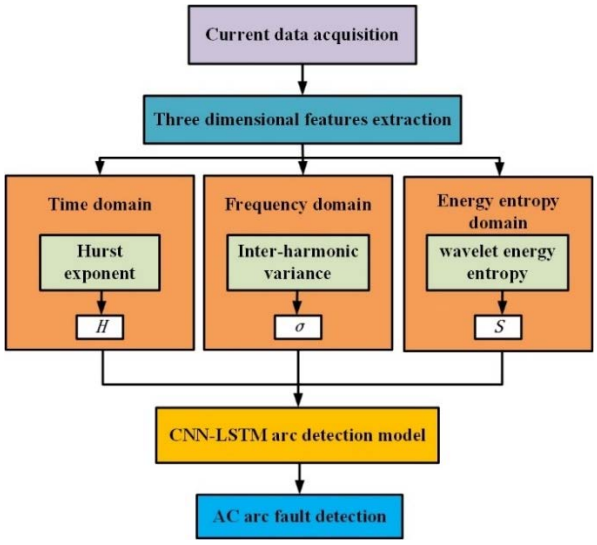

FIGURE 8. Arc fault detection scheme.

IV. ARC FAULT FEATURE EXTRACTION

Traditional arc fault detection methods are often used to analyze a certain characteristic of arc signals, but it is difficult

to achieve the same detection effect on different types of arc faults with these methods. Therefore, in order to break through the limitations of traditional arc signal feature extraction methods and achieve effective detection of different types of AC arc faults, the time-frequency-energy of the signals is analyzed based on the short-time Fourier transform (STFT) in this section. The two-dimensional distribution of time-frequency-energy provides the basis for the selection of three-dimensional features of arc signals. Then, the H-I-W three-dimensional features are extracted with an improved algorithm and used as the feature data basis for fault detection.

A. STFT AND FEATURE SELECTION ANALYSIS

As a combination of fast Fourier transform and time window, STFT is mainly used to determine the frequency and phase of the signal in a local area. The primary method is to select a time-frequency local window function $h(t)$. It is assumed that $h(t)$ is stationary in a short time interval. Then, $h(t)$ moves in such a way that $x(t)h(t)$ is a stationary signal in different finite times. Finally, the power spectrum is calculated at different finite times. The discrete STFT equation is provided below:

$$STFT(\tau, f; h) = \sum_{t_1}^{t_2} x(t)h(t-\tau)e^{-j2\pi ft}\Delta t, \qquad (1)$$

where τ is the moving distance of the window function; f is the sampling frequency; $[t_1, t_2]$ is the sampling interval; $x(t)$ is the sampling current; Δt is the sampling time step.

In order to clearly display the energy distribution trend in the time-frequency domain, energy is calculated as:

$$E(\tau, f; h) = 10\log|STFT(\tau, f; h)|^2. \qquad (2)$$

Discrete short-time Fourier transform is performed on the test current shown in Fig. 6. Its energy is calculated and the time, frequency, and energy distributions are plotted in a two-dimensional coordinate system, as shown in Fig. 9.

When an arc occurred, the time-frequency-energy distribution of the current was obviously different from that under the normal state at the location where the arc occurred (Fig. 9). The combination of time domain, frequency domain, and energy clearly highlighted the unique characteristics of an arc. Therefore, in this paper, the features were extracted respectively from the time domain, frequency domain, and energy domain and then combined together to obtain three-dimensional features for arc fault detection. However, the combinations of too many features limit generalizability and lead to overfitting and fewer feature combinations lead to the loss of a lot of information. Therefore, in this paper, based on a large number of experimental simulation data and the real-time detection requirement in UL1699 standard, a feature was respectively selected in the time domain, frequency domain, and energy domain and combined together in order to achieve effective detection of arc faults.

In the time domain, compared with the representative indicators such as kurtosis, skewness, and form factor, the Hurst exponent introduced in this paper can better reflect the

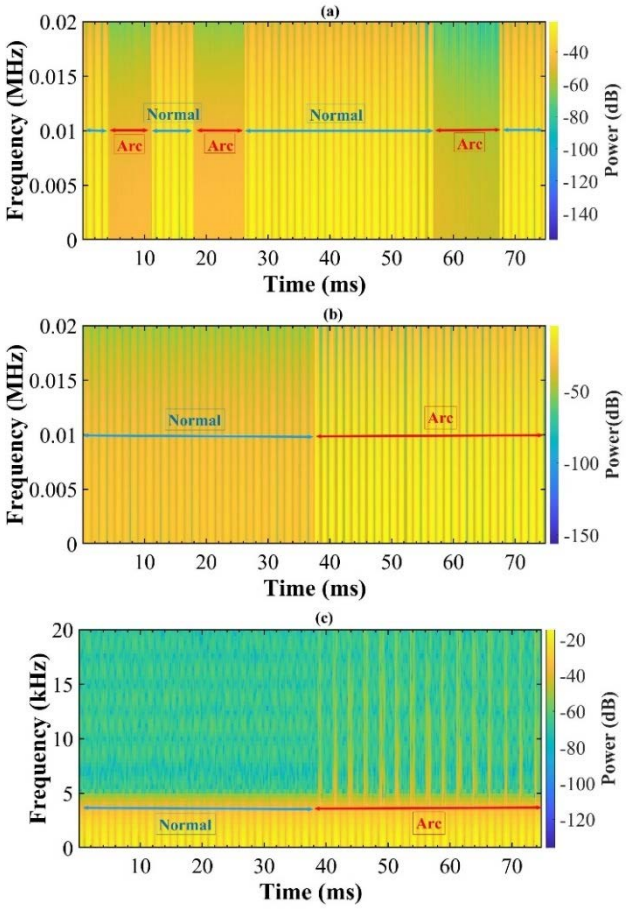

FIGURE 9. Time-frequency-energy distributions of arc test current: (a) vibration test, (b) cutting test, and (c) wet arc trajectory test.

characteristics of the current. In the frequency domain, the centroid frequency, the mean square frequency, and the root mean square frequency all described the position distribution of the main frequency band of the power spectrum, but they were not suitable for arc fault detection. Furthermore, the ability of inter-harmonic variance to identify partial changes in signal frequency was better than that of the inter-harmonic mean value, 3rd harmonic amplitude and 5th harmonic amplitude. Therefore, in this paper, the inter-harmonic variance was selected as the frequency domain feature. In the energy domain, the wavelet stratification and the spatial distribution analysis of energy entropy contributed to the extraction of weak features of arcs, so wavelet energy entropy was chosen to detect arc faults.

B. HURST EXPONENT FEATURE EXTRACTION

The Hurst exponent is a biased random walk proposed by Hurst and widely applied in environmental variable prediction, nonlinear analysis of the stock market, tool wear monitoring, cemented carbide drilling fault monitoring, and DC arc detection of vehicles [27], but it has not yet been applied in the AC arc fault detection of aviation cables. The main

methods of extracting the Hurst exponent in this paper are introduced as follows:

Firstly, for a given time series $x(i)$ with the length, N, $x(i)$ is divided into M subsequences with the length n. The mean $\mu_{n,m}$ of the subsequences is expressed as:

$$\mu_{n,m} = \frac{1}{n}\sum_{i=1}^{n} x(i,m), \tag{3}$$

where $x(i,m)$ is the i-th data in the m-th subsequence of the signal and $m = 1, 2, \ldots, M$.

The mean adjustment sequence is defined as follows:

$$D_{i,m} = x(i,m) - \mu_{n,m}, \quad i = 1, 2, \ldots, n. \tag{4}$$

The cumulative dispersion $Z_{i,m}$ of the subsequence is expressed as:

$$Z_{i,m} = \sum_{j=1}^{i} D_{j,m}, \quad i = 1, 2, \ldots, n. \tag{5}$$

Secondly, the subsequence range $R_d$is calculated as:

$$R_d = \max_{1\le i\le n}\{Z_{i,m}\} - \min_{1\le i\le n}\{Z_{i,m}\}. \tag{6}$$

Thirdly, the standard deviation S_d of the subsequence is calculated as:

$$S_d = \sqrt{\frac{1}{n}\sum_{i=1}^{n}(x(i,m) - \mu_{n,m})^2}. \tag{7}$$

Fourthly, the mean R/S for each rescaling range R_d/S_d and all M subsequence rescaling ranges is calculated as:

$$R/S = \frac{1}{M}\sum_{m=1}^{M} R_d/S_d. \tag{8}$$

Finally, the Hurst exponent of the subsequence is calculated as:

$$\log\frac{R}{S} = H\log n + \log C, \tag{9}$$

where H is the Hurst exponent and C is a constant. Taking the current signal per cycle as a time series, the size of the time window n is N, $N/2$, $N/4$, $N/6$, $N/8$, and $N/10$ in turn and the calculation steps of Equation (3) to Equation (8) are repeated.

The slope H is estimated by linear regression with 6 different values of n. In the value range of H, [0, 1], when $0 \le H < 0.5$, the time series is pink noise and its power spectral density is inversely proportional to the frequency; when $H = 0.5$, the time series is a random walk and the future trend cannot be predicted with existing data; when $0.5 < H < 1$, the time series is chaotic and future variable changes can be predicted with existing data; when $H = 1$, the time series is a straight line.

The Hurst exponent is calculated for the three test currents, as shown in Fig. 10.

Before the arc occurred, the Hurst exponent of the current was close to 1 and the currents in adjacent cycles were correlated with each other (Fig. 10). When an arc fault occurred, the value of the Hurst exponent decreased sharply and the Hurst exponent waveform fluctuation range was greatly increased. These changes might be interpreted as follows. The occurrence of the arc decreased the correlation between the currents at adjacent moments, so the randomness of the Hurst exponent distribution per cycle increased. It was found that the value of Hurst exponent of the arc cycle was smaller than that in the normal state. The value of Hurst exponent was always greater than 0.5, so the Hurst exponent could be used to predict the occurrence of future arc faults.

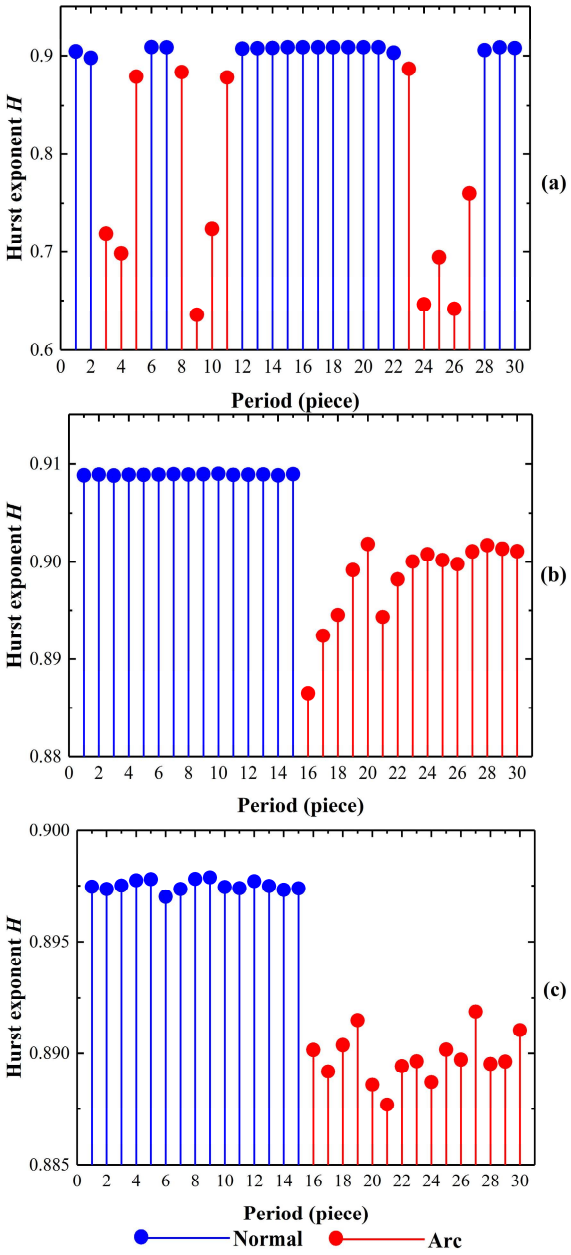

FIGURE 10. Hurst exponent of arc test current in various tests: (a) vibration test, (b) cutting test, and (c) wet arc trajectory test.

C. INTERHARMONIC VARIANCE FEATURE EXTRACTION

The frequency-domain method is a signal analysis method with the good real-time performance. It mainly diagnoses and detects a fault based on the fluctuation of the content of signal

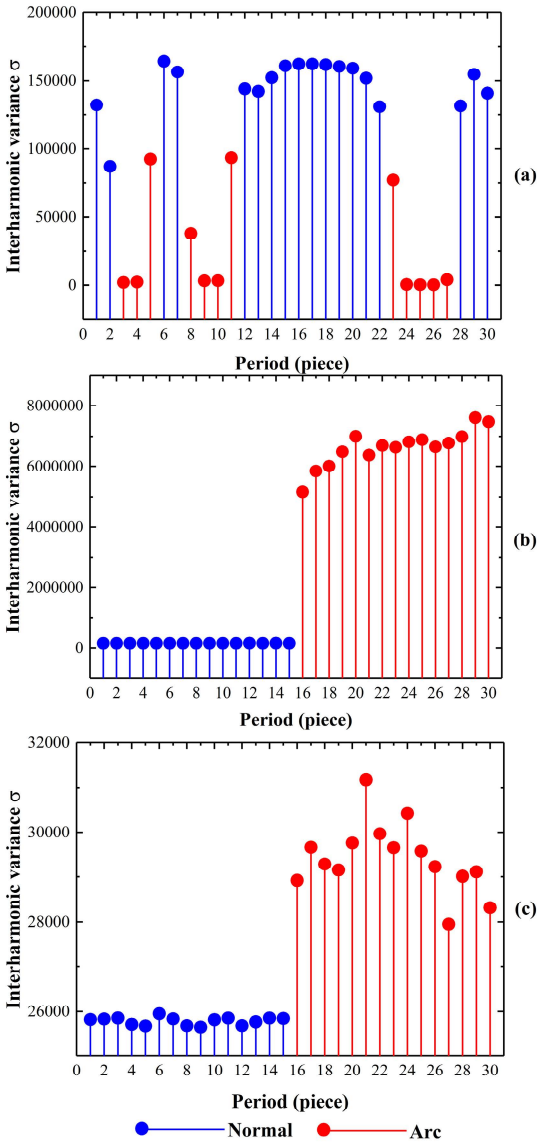

FIGURE 11. Inter-harmonic variance of arc test current in various tests: (a) vibration test, (b) cutting test, and (c) wet arc trajectory test.

component and its detection result has good reliability. The main methods of extracting inter-harmonic variance in this paper are described as follows:

Firstly, the discrete Fourier transform $X(k)$ of the time series $x(i)$ is calculated as:

$$X(k) = \sum_{i=1}^{N} x(i) e^{-j\frac{2\pi}{N}}, \tag{10}$$

where $k = 1, 2, \ldots, N$ and N is the length of time series.

The intermediate harmonic components of $X(k)$ are selected to form a new set $X_1(k)$ of discrete Fourier transforms.

Then, the inter-harmonic mean value $\bar{X}_1(k)$ of the time series is calculated as:

$$\bar{X}_1(k) = \frac{1}{N_1} \sum_{k=1}^{N_1} X_1(k), \tag{11}$$

where N_1 is the length of $X_1(k)$.

Finally, the inter-harmonic variance σ of the time series is calculated as:

$$\sigma = \frac{1}{N_1} \sum_{k=1}^{N_1} (X_1(k) - \bar{X}_1(k))^2. \tag{12}$$

The above frequency domain analysis is performed with the three test currents shown in Fig. 6 and the inter-harmonic variance of each cycle of the current is respectively calculated (Fig. 11).

Before an arc occurred, the distribution of the inter-harmonic variance of currents was approximately a horizontal line (Fig. 11). When an arc occurred, the current inter-harmonic variance in the vibration test decreased instantaneously and its value was close to 0. The current inter-harmonic variance in the cutting test and the wet arc trajectory test increased abruptly and the fluctuation degree of the curve increased greatly. These changes might be interpreted as follows. The cable was separated from the terminal for a short time in the vibration test. In addition, due to the short circuit between lines, the current deviation degree in the cutting test and the wet arc trajectory test became larger.

It was found that the inter-harmonic variance of the current in the case of an arc was changed by an order of magnitude above 10^4. Therefore, the inter-harmonic variance was used as the frequency domain feature for detecting arc faults in this paper.

D. WAVELET ENERGY ENTROPY FEATURE EXTRACTION

Wavelet transform is an effective tool to deal with non-stationary signals. Wavelet transform can be used to analyze the signal at different scales and the sectional characteristics of the signal with a better time-frequency window and realize the detection of transient mutation and singularity of the signal.

Information entropy is a measure to describe the complexity and uncertainty of a signal. The change in entropy indicates the change in the degree of uncertainty of a signal. Therefore, wavelet energy entropy is an important method of analyzing signal uncertainty in information entropy. Wavelet energy entropy reflects the energy distribution of signals at different scales. The main calculation methods of wavelet energy entropy in this paper are introduced as follows:

Firstly, the energy of the i-th sampling point of the time series at the a scale is defined as $E_a(i)$. The total energy of the time series at the a scale is expressed as:

$$E(a) = \sum_{i=1}^{N} E_a(i). \tag{13}$$

Then, the total energy E of the signal is calculated as:

$$E = \sum_{a=1}^{m} E(a). \tag{14}$$

where m is the number of dimension layers under wavelet transform.

Finally, let $p_a = E(a)/E$. The energy entropy of the wavelet under the scale a is:

$$S = -\sum_{a=1}^{m} p_a \log p_a. \tag{15}$$

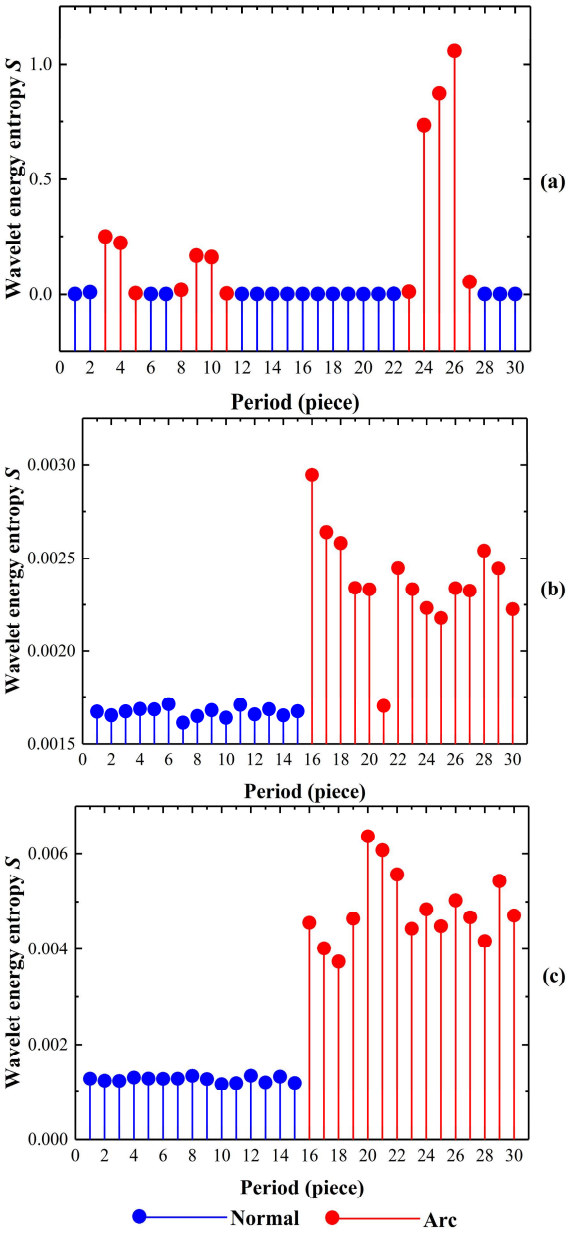

FIGURE 12. Wavelet energy entropy of arc test current in various tests: (a) vibration test, (b) cutting test, and (c) wet arc trajectory test.

The wavelet energy entropy S is calculated based on the current shown in Fig. 6 and the calculation result is shown in Fig. 12.

Before the occurrence of an arc, the entropy curve of the current was basically a horizontal line and the fluctuation was small (Fig. 12). When an arc occurred, the wavelet energy entropy of the current in the vibration test was increased greatly; the wavelet energy entropy of the current in the cutting test was increased by 1.344 to 1.875 times; the wavelet energy entropy of the current in the wet arc trajectory test was increased by 2.230 to 3.875 times. Therefore, when an arc occurred, the wavelet energy entropy changed significantly, indicating that this feature could be used to identify the arc fault.

TABLE 2. H-I-w features of wet arc trajectory test.

Features	States	Periods	Load 1	Load 2	Load 3	Load 4
H	Common	1	0.8976	0.9217	0.9158	0.9012
		2	0.8975	0.9213	0.9134	0.8962
		3	0.8977	0.9215	0.9145	0.8924
	Fault	16	0.8905	0.6529	0.8014	0.6005
		17	0.8889	0.5962	0.7968	0.6435
		18	0.8908	0.6637	0.7988	0.5832
$I/10^4$	Common	1	2.5989	3.6585	2.6320	3.8989
		2	2.5891	3.6625	2.6547	3.6891
		3	2.5905	3.6405	2.6464	3.9905
	Fault	16	2.8907	4.7750	2.8996	5.5248
		17	2.9765	5.6129	3.0856	4.8759
		18	2.9524	4.6782	3.0045	5.8908
$W/10^{-3}$	Common	1	1.2453	1.4657	1.3045	2.5823
		2	1.1856	1.4114	1.2376	2.5837
		3	1.1857	1.4382	1.2857	2.5856
	Fault	16	5.1578	5.5789	4.4317	10.6487
		17	4.0223	6.6893	4.8446	11.2568
		18	3.8486	8.6621	5.0295	9.2267

E. FEATURE EXTRACTION ANALYSIS UNDER DIFFERENT LOADS

In order to fully simulate the different circuit conditions in the case of a cable arc, arc currents under different loads were collected and analyzed, and the H-I-W three-dimensional characteristics were calculated respectively under different loads. Taking the wet arc trajectory test as an example, some calculation results are shown in Table 2.

When an arc occurred, the capacitive load, inductive load, and nonlinear load in the wet arc trajectory test could lead to more obvious characteristic changes (Table 2). Under non-resistive loads, the occurrence of arcs tended to be more random and unpredictable because the fractal characteristics of the current became weaker and the Hurst exponent decreased. Due to the enhanced randomness and unpredictability, the stability of the current became worse and both the harmonic variance and the wavelet energy entropy increased exponentially.

The H-I-W three-dimensional features were extracted respectively from the currents of the cutting test and the vibration test under different types of load conditions. The analysis and comparison results showed that the H-I-W three-dimensional features changed significantly when an arc occurred. Statistical analysis results of multiple tests showed that, in the same type of arc test, after an arc occurred, the H-I-W three-dimensional feature of the current showed a stable change direction. In a word, the H-I-W three-dimensional feature could be used to identify the occurrence of AC arc faults.

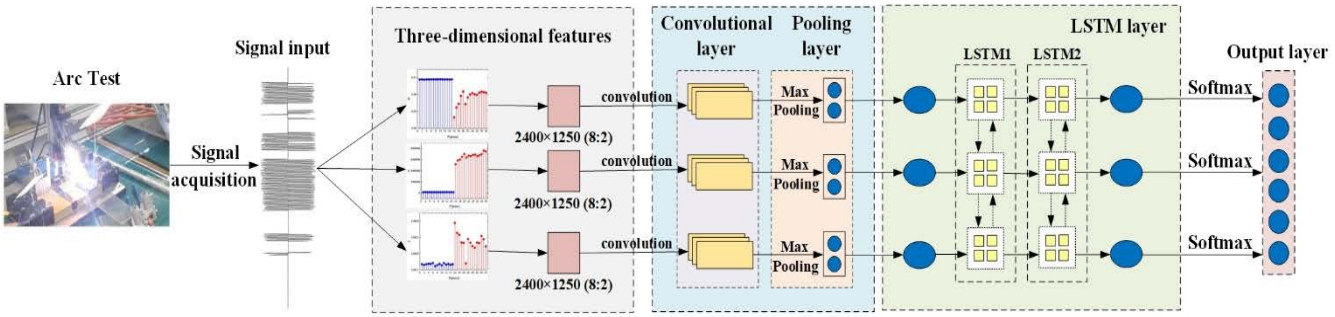

FIGURE 13. AC arc fault detection model of aviation cables.

V. ARC FAULT DETECTION BASED ON CNN-LSTM

The occurrence of an arc fault is random and uncertainty and the arc fault may be affected by the type of load and wiring, so it is difficult to identify the arc fault flexibly and efficiently in different working environments only through manually setting thresholds. A feasible method of accurately identifying arc faults is to grasp the changes of the characteristic behavior with intelligent identification algorithms.

Arc intelligent recognition algorithms include BP neural network (BPNN), SVM [26], DNN [29], RNN [32], CNN [33], LSTM [36], and CNN-LSTM. Among them, CNN-LSTM combines the advantages of CNN and LSTM with space invariance and time invariance, so it shows more advantages in dealing with time series and complex data. Therefore, the arc fault detection model was established based on CNN-LSTM in the study.

A. FAULT DETECTION MODEL AND PROCESS

The AC arc fault detection model of aviation cables based on CNN-LSTM is shown in Fig. 13. The model is mainly composed of an arc test, signal input layer, signal feature extraction layer, convolution layer and pooling layer of CNN, LSTM layer, and classification output layer. The core of the model includes signal feature extraction, training and testing with hybrid neural network, and fault identification.

In this paper, the arc fault detection process based on H-I-W three-dimensional features and CNN-LSTM hybrid neural network is introduced below:

1) Through the arc test, the arc current is collected and saved and the current state is calibrated according to the standard SAE AS5692A;
2) After the time window is determined, the H-I-W three-dimensional features of the current signal are extracted. Each feature is filled into a two-dimensional matrix of 2400 × 1250 so as to form 3 groups of feature datasets with the size of 2400 × 1250. In the feature dataset, 2400 is the number of feature rows for three arc tests under four types of loads and 1250 is the manually set number of features in each row;
3) The training set (1920 × 1250) and the test set (480 × 1250) are divided according to the ratio of 8:2 and the dataset is labeled according to the state calibration in 1);
4) The optimal initial parameters of the model were found with the grid search algorithm and the batch size, learning rate, iteration number W, and initialization training number $v = 1$ of the CNN-LSTM network are set;
5) The training set is input into the convolution layer of the CNN network and the secondary features are adaptively extracted through the convolution kernel. Then the secondary features are input into the pooling layer for maximum pooling operation, which can reduce the feature dimension and retain the main feature information;
6) The dimensionality reduction feature data output by the CNN network are input into the LSTM layer in the training process of the LSTM network and the feature learning process;
7) The model parameters are updated with the error calculation back-propagation algorithm and the signals are classified with the Softmax function;
8) Whether the number of training v reaches the preset number of iterations W is determined. If it reaches the preset number, go to the next step, otherwise return to Step 5 to continue the iteration;
9) The test set is input into the CNN-LSTM network to test the performance of the model. Fault identification accuracy is calculated and the calculation result is output. Finally, the calculation ends.

The detailed process of AC arc fault detection in aviation cables is shown in Fig. 14.

B. NETWORK PARAMETER SETTINGS

Parameter setting is crucial to the training and testing results of neural network. Based on the consideration of the characteristics of arc data, the hyperparameters are selected with the exhaustive method and the final CNN-LSTM network parameters are set as follows:

1) CNN is designed with 5 convolutional layers. The kernel size of the convolutional layer is 3 × 3 and the activation function is ReLU. The filling method is the same and the numbers of the channels in 5 layers are 16, 16, 64, 64, and 128, respectively.

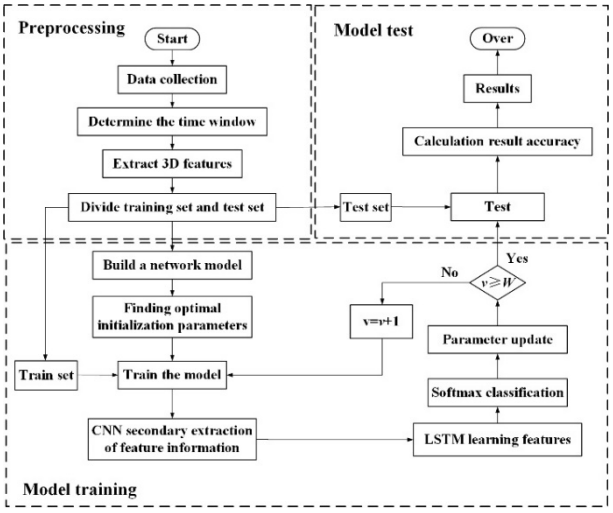

FIGURE 14. Flow chart of arc fault detection based on CNN-LSTM.

2) CNN has 5 pooling layers. The kernel size of the pooling layer is 1×1 and the numbers of the channels of 5 layers are 16, 16, 64, 64, and 128, respectively. The pooling layer adopts the maximum pooling method in order to avoid the shift in the mean estimate caused by small changes in the convolution kernel.
3) LSTM uses a two-layer network to learn feature sequence information. The number of neural networks is 128 and the activation function is Tanh. Boundary part are filled with 0 in order to ensure that the output size does not change.
4) The activation function of the Softmax layer is softmax.
5) The kernel size of the output layer is 2. The number of channels is 1 and the output size is 2.
6) The optimal initial learning rate of 0.0001 is selected with the grid search algorithm. The batch size is 800 and the number of iterations $W = 2000$. Adam optimization algorithm is used to optimize the model.

In the parameter setting process, the ReLU function can increase the network sparsity compared with the Sigmoid function and Tanh function, thus endowing the network with the better generalization ability. The batch size is adjusted to train CNN-LSTM. When the batch size is 800, CNN-LSTM has fast training speed and high detection accuracy. Therefore, the batch size of 800 is the optimal choice. Furthermore, H-I-W features for each of the three tests under four loads of current are extracted and then each feature is filled in a 2400×1250 matrix to form a feature data set. Thus, each group of data set contains three arc tests and four loads. The designed arc detection model has the good generalization ability.

In addition, ReLU reduces the computation load and the dependency between parameters so as to accelerate the convergence and mitigate the overfitting problem. The pooling layer reduces the number of parameters through maximum pooling in order to prevent the CNN-LSTM network from overfitting. Therefore, the CNN-LSTM model can detect faults without overfitting.

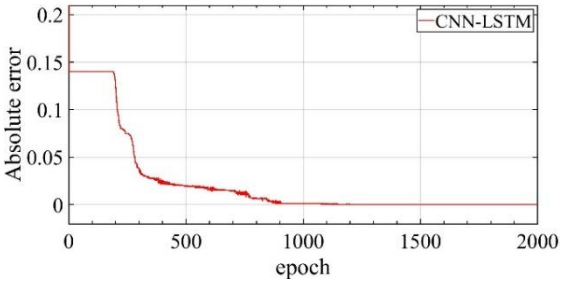

FIGURE 15. Absolute error of CNN-LSTM network model training.

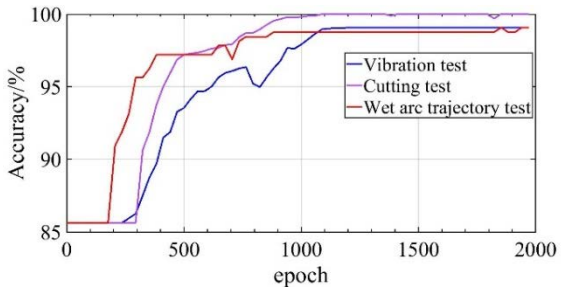

FIGURE 16. Test accuracy of AC arc fault detection model.

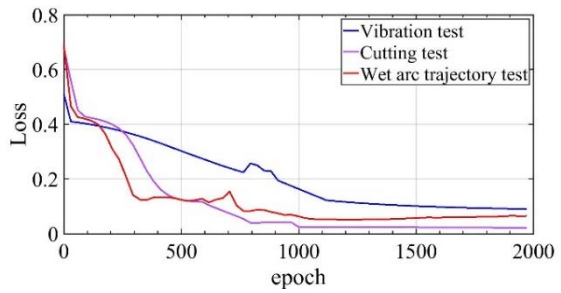

FIGURE 17. Test loss of AC arc fault detection model.

C. FAULT DETECTION RESULTS

The training set is used to train the aviation cable fault detection model and the absolute error of network training is shown in Fig. 15.

When the number of iterations was small, the absolute error of network training is above 0.14 (Fig. 15). When the number of iterations exceeded 189, the absolute error of the model decreased. As the number of iterations increased, the rate of absolute error reduction gradually decreased. When the number of iterations reached 1200, the absolute error converged to 0. In this way, the network model was successfully trained.

The vibration test set, cutting test set, and wet arc trajectory test set of the same size were respectively input into the trained CNN-LSTM neural network model for testing. The accuracy and loss of the model test are respectively shown in Fig. 16 and Fig. 17.

Due to the obvious change in the characteristics of the cutting test, when the number of iterations exceeded 1200, the fault detection accuracy was as high as 100% (Fig. 16). The detection accuracy of the arc fault in both the vibration test and wet arc trajectory test was above 98.74%. When the number of iterations exceeded 1200, the loss of the model test converged to the minimum value and the loss value was 0.021 to 0.09 (Fig. 17).

Arc fault detection tests were repeatedly under different types of loads. After 2000 iterations, the fault detection accuracy was obtained (Table 3). Arc fault detection accuracy in the three tests under different loads was above 98.11%, indicating that the method in this paper could effectively identify and detect arc faults under different loads. The comprehensive average detection accuracy rate was 98.75%.

In order to verify the advantages of the combined H-I-W features, we did not use one or two of the H-I-W three-dimensional features for arc fault detection. The results showed that the detection accuracy decreased when one or two of the H-I-W three-dimensional features were not used. Detection accuracy was decreased by 9.19% to 11.52% when two of the H-I-W three-dimensional features were not used. Detection accuracy was decreased by 4.24% to 6.40% when one of the H-I-W three-dimensional features was not used. Therefore, H-I-W features combined the advantages of three features and overcame the shortcomings of single feature detection. H-I-W contributed greatly to the improvement in arc fault detection accuracy.

In the arc fault detection process, the extraction time of Hurst exponent, inter-harmonic variance, and wavelet energy entropy was respectively shorter than 0.059 s, 0.027 s, and 0.359 s. The extraction time of H-I-W three-dimensional feature was shorter than 0.445 s. It took less than 0.545 s to input H-I-W three-dimensional feature data into CNN-LSTM for arc fault detection. Therefore, the arc fault detection could be completed within 0.99 s, which met the real-time detection requirement for the current level of 5 A in UL1699 standard. Under the sampling rate of 500 KHz, the method proposed in this paper for the three AC arc faults realized the average detection accuracy of 98.44% and detection time of 0.132 s, which met real-time requirements for 5 A, 10 A, and some other current levels in UL1699 standard. All calculations in the paper were completed on a DELL notebook (CPU i7-7500), so the proposed method could be implemented on embedded platform like JETSON TX2. JETSON TX2 has 8 GB RAM, 59.7 GB/s memory bandwidth, and NVIDIA Pascal GPU with 256 NVIDIA CUDA cores, which endow JETSON TX2 with excellent neural network algorithm processing capability.

In the actual aircraft power control system, the load circuit current was collected by SSPC in real time and then transmitted to the CPU in the Electrical Load Management Center (ELMC) via the bus for status monitoring, and the ELMC then controlled the work of SSPC through feedback commands, thus realizing real-time management of the load circuit. The internal structure of ELMC is shown in Fig. 18.

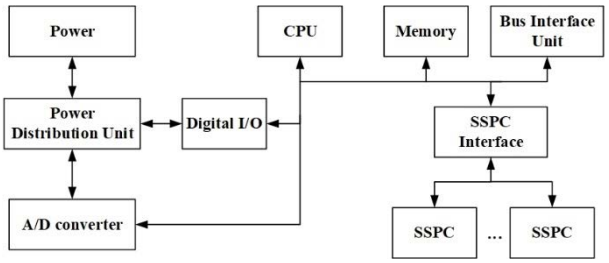

FIGURE 18. Internal structure sketch of ELMC.

Therefore, the method proposed in this paper could be applied in the CPU of the ELMC so as to monitor the arc faults in aviation cables in real time. In addition, actual appliances can adopt lower sampling rates (500 KHz) or neural-network processing unit (NPU) so as to reduce the computational cost and increase the detection speed.

D. COMPARATIVE ANALYSIS

The proposed method in this paper is compared with advanced methods in terms of method principle, feature combination, test type, maximum detection time, and average detection accuracy. The comparison results are shown in Table 4.

Bao *et al.* [13] used a fourth-order cumulative volume algorithm to detect arc pulses at a sampling rate of 10 MHz, but the method could not distinguish normal pulses from arc pulses. Jiang *et al.* [14] combined regular coupling features (RCFs) with SVM to determine the presence of arcs by impulse factor analysis (IFA) and then trained the SVM to further identify arc pulses and normal pulses by covariance matrix analysis (CMA) and multiple frequency-band analysis (MFA). This method successfully differentiated normal pulse signals from arc fault pulse signals and reduced the misidentification rate. However, in the vibration test and wet arc trajectory test, when an arc fault occurred, current pulses were scarce and the value of IFA was slightly changed, thus causing mistaken detection of arc faults. Qu *et al.* [4] achieved accurate load classification by extracting a large number of features and learning vector quantization neural network (LVQ-NN), and accomplished arc fault identification by support vector machines optimized by particle swarm optimization (PSO-SVM), but the method spent longer time in achieving these results. Yang *et al.* [35] converted the normalized one-dimensional data into two-dimensional data and then two-dimensional grayscale image, obtained the target image by filtering and finally input it into CNN for recognition. The method could identify the arc fault more accurately, but it required so many computing equipment that it was difficult to be applied in CPU. In this paper, three arc tests were designed based on the actual induction factors of arc faults so as to acquire more accurate simulation results. The previous methods [4], [13], [14], and [35] were used to detect vibrating arc, cutting arc, and wet arc trajectory arc faults, respectively. The detection accuracy of vibration

TABLE 3. AC Arc fault detection accuracy under different loads.

Loads	Load 1	Load 2	Load 3	Load 4	Average
Vibration test	99.06%	98.32%	98.58%	98.11%	98.52%
Cutting test	100.00%	99.13%	99.26%	98.54%	99.23%
Wet arc trajectory test	98.75%	98.47%	98.62%	98.21%	98.51%

TABLE 4. Comparison between the proposed method and previous advanced detection methods.

Sources	Guanghai Bao [13]	Na Qu [4]	Run Jiang [14]	Kai Yang [35]	This paper
Methods	High-order cumulants	LVQ-NN and PSO-SVM	RCFs and SVM	TDV and CNN	CNN-LSTM
Features	Kurtosis	4 time-domain and 10 frequency-domain	IFA+CMA+MFA	Two-dimensional grayscale images	H-I-W
Arc test types	Point contact test	Point contact test	Point contact test	Point contact test	Vibration test, Cutting test, Wet arc trajectory test
Ave. detection accuracy	80.6%	97.58%	99.4%	98.7%	98.56%

test arc fault of the two previous methods [13] and [14] was below 80% and the detection time of two methods [4] and [35] exceeded 1 s. The method proposed in this paper first extracted the H-I-W, then the input it into CNN-LSTM for arc fault detection, and finally achieved effective and fast AC arc fault detection. Even under sampling rate of 500 KHz, the average arc fault detection accuracy were still above 98.4% and the detection speed met real-time requirements for most of current levels in UL1699 standard.

VI. CONCLUSION

In this paper, three kinds of AC arc tests were carried out based on the standard SAE AS5692A. After the occurrence of AC arc faults, the current waveform changed to different degrees and the difference between the fault current waveform and the normal current waveform in the wet arc track test was the smallest. The two-dimensional time-frequency-energy distribution of the current indicated that the combination of time domain, frequency domain, and energy entropy could highlight arc faults and enhance the fault identification ability. The arc fault detection method integrating H-I-W three dimensional features with CNN-LSTM neural network showed their combined advantages. The following conclusions were drawn from the test data:

Firstly, the arc fault specific triggering factors were analyzed and based on the standard SAE AS5692A, the vibration arc test, cutting arc test, and wet arc trajectory arc test were designed to overcome the limitation of the traditional point contact test.

Secondly, the introduced Hurst exponent could identify and predict the occurrence of AC arc faults. The H-I-W three-dimensional feature showed the combined advantages of time domain, frequency domain, and energy entropy and further improved the detection accuracy and robustness of the proposed method.

Thirdly, compared with four advanced methods, the method proposed in this paper showed the better real-time detection performance and the average detection accuracy of 98.56% and realized the fast and effective detection of AC arc faults in aviation cables.

Fourthly, the feature extraction algorithm and CNN-LSTM structure proposed in this paper were simple and met the real-time detection requirements in UL1699 standard. The proposed method can be applied in an actual aviation application environment and has a certain engineering value in the detection of AC arc faults in aviation cables.

REFERENCES

[1] P. Wu, B. Ming, and Q. Wang, "Online aviation cable fault detection based on spread spectrum time domain reflectometry," in *Proc. IEEE 5th Int. Conf. Comput. Commun. (ICCC)*, Chengdu, China, Dec. 2019, pp. 976–980.
[2] J. Andrea, "Génération, modélisation et détection des défauts d'arc électrique: Application aux systèmes embarqués aéronautiques," Tech. Rep., May 2011.
[3] K. Lyu, Q. Li, Z. Zhu, J. Qiu, and G. Liu, "Mechanism analysis and dynamic model construction of intermittent fault of weak-current aviation cable under vibration stress," *Adv. Mech. Eng.*, vol. 14, no. 3, pp. 1–13, Mar. 2022.
[4] N. Qu, J. Zuo, J. Chen, and Z. Li, "Series arc fault detection of indoor power distribution system based on LVQ-NN and PSO-SVM," *IEEE Access*, vol. 7, pp. 184020–184028, 2019.
[5] J. Andrea, O. Zirn, and M. Bournat, "Principle of arc fault detection for solid state power controller," in *Proc. IEEE 58th Holm Conf. Electr. Contacts (Holm)*, Portland, OR, USA, Sep. 2012, pp. 1–6.
[6] J. Jiang, M. Zhao, Z. Wen, C. Zhang, and R. Albarracín, "Detection of DC series arc in more electric aircraft power system based on optical spectrometry," *High Voltage*, vol. 5, no. 1, pp. 24–29, Aug. 2019.
[7] X. Yu and H. Su, "Pantograph arc detection of urban rail based on photoelectric conversion mechanism," *IEEE Access*, vol. 8, pp. 14489–14499, 2020.
[8] Y. Ke, W. Zhang, C. Suo, Y. Wang, and Y. Ren, "Research on low-voltage AC series arc-fault detection method based on electromagnetic radiation characteristics," *Energies*, vol. 15, no. 5, p. 1829, Jan. 2022.
[9] A. Mukherjee, A. Routray, and A. K. Samanta, "Method for online detection of arcing in low-voltage distribution systems," *IEEE Trans. Power Del.*, vol. 32, no. 3, pp. 1244–1252, Jun. 2017.
[10] A. F. Sultan, G. W. Swift, and D. J. Fedirchuk, "Detecting arcing downed-wires using fault current flicker and half-cycle asymmetry," *IEEE Trans. Power Del.*, vol. 9, no. 1, pp. 461–470, Jan. 1994.
[11] J. Lezama, P. Schweitzer, E. Tisserand, J.-B. Humberta, S. Webera, and P. Joyeux, "An embedded system for AC series arc detection by inter-period correlations of current," *Electr. Power Syst. Res.*, vol. 129, pp. 227–234, Dec. 2015.

[12] J. Lezama, P. Schweitzer, S. Weber, E. Tisserand, and P. Joycux, "Arc fault detection based on temporal analysis," in *Proc. IEEE 60th Holm Conf. Electr. Contacts (Holm)*, New Orleans, LA, USA, Oct. 2014, pp. 1–5.
[13] G. Bao, R. Jiang, and D. Liu, "Research on series arc fault detection based on higher-order cumulants," *IEEE Access*, vol. 7, pp. 4586–4597, 2019.
[14] R. Jiang, G. Bao, Q. Hong, and C. Booth, "Machine learning approach to detect arc faults based on regular coupling features," *IEEE Trans. Ind. Informat.*, early access, Feb. 23, 2022, doi: 10.1109/TII.2022.3153333.
[15] R. Jiang, G. Bao, Q. Hong, and C. D. Booth, "A coupling method for identifying arc faults based on short-observation-window SVDR," *IEEE Trans. Instrum. Meas.*, vol. 70, pp. 1–10, 2021.
[16] R. Jiang and Y. Zheng, "Series arc fault detection using regular signals and time-series reconstruction," *IEEE Trans. Ind. Electron.*, early access, Apr. 12, 2022, doi: 10.1109/TIE.2022.3165260.
[17] H. Guan, B. Wang, Z. Zhao, S. Bimenyimana, and Q. Wang. (2016). *Arc Fault Current Signal's Power Spectrum Characteristics and Diagnosis Based on Welch Algorithm*. [Online]. Available: https://www.semanticscholar.org
[18] F. M. Uriarte, A. L. Gattozzi, J. D. Herbst, H. B. Estes, T. J. Hotz, A. Kwasinski, and R. E. Hebner, "A DC arc model for series faults in low voltage microgrids," *IEEE Trans. Smart Grid*, vol. 3, no. 4, pp. 2063–2070, Dec. 2012.
[19] J. Lezama, P. Schweitzer, S. Weber, E. Tisserand, P. Joyeux, and M. Rabla, "Frequency analysis to arcing detection and prototyping FPGA approach," in *Proc. IEEE 59th Holm Conf. Electr. Contacts (Holm)*, Newport, RI, USA, Sep. 2013, pp. 1–6.
[20] M. Atharparvez and K. R. Purandare, "Series arc fault detection using novel signal processing technique," in *Proc. IEEE Holm Conf. Electr. Contacts*, Albuquerque, NM, USA, Oct. 2018, pp. 335–339.
[21] W. Li, K. He, W. Liu, X. Zhang, and Y. Dong, "A fast arc fault detection method for AC solid state power controllers in MEA," *Chin. J. Aeronaut.*, vol. 31, no. 5, pp. 1119–1129, May 2018.
[22] G. Artale, A. Cataliotti, V. Cosentino, D. Di Cara, S. Nuccio, and G. Tiné, "Arc fault detection method based on CZT low-frequency harmonic current analysis," *IEEE Trans. Instrum. Meas.*, vol. 66, no. 5, pp. 888–896, May 2017.
[23] E. Karakose, M. T. Gencoglu, M. Karakose, O. Yaman, I. Aydin, and E. Akin, "A new arc detection method based on fuzzy logic using S-transform for pantograph–catenary systems," *J. Intell. Manuf.*, vol. 29, no. 4, pp. 839–856, Aug. 2015.
[24] C. Chen, F. Guo, Y. Liu, Z. Wang, Y. Chen, and H. Liang, "Recognition of series arc fault based on the Hilbert Huang transform," in *Proc. IEEE 61st Holm Conf. Electr. Contacts (Holm)*, San Diego, CA, USA, Oct. 2015, pp. 324–330.
[25] P. Qi, S. Jovanovic, J. Lezama, and P. Schweitzer, "Discrete wavelet transform optimal parameters estimation for arc fault detection in low-voltage residential power networks," *Electr. Power Syst. Res.*, vol. 143, pp. 130–139, Feb. 2017.
[26] S. H. Mortazavi, Z. Moravej, and S. M. Shahrtash, "A hybrid method for arcing faults detection in large distribution networks," *Int. J. Electr. Power Energy Syst.*, vol. 94, pp. 141–150, Jan. 2018.
[27] Y. Abdullah, J. Shaffer, B. Hu, B. Hall, J. Wang, A. Emrani, and B. Arfaei, "Hurst-exponent-based detection of high-impedance DC arc events for 48-V systems in vehicles," *IEEE Trans. Power Electron.*, vol. 36, no. 4, pp. 3803–3813, Apr. 2021.
[28] Y. Wang, F. Zhang, and S. Zhang, "A new methodology for identifying arc fault by sparse representation and neural network," *IEEE Trans. Instrum. Meas.*, vol. 67, no. 11, pp. 2526–2537, Nov. 2018.
[29] J. Jiang, W. Li, Z. Wen, Y. Bie, H. Schwarz, and C. Zhang, "Series arc fault detection based on random forest and deep neural network," *IEEE Sensors J.*, vol. 21, no. 15, pp. 17171–17179, Aug. 2021.
[30] A. Amiri, H. Samet, and T. Ghanbari, "Recurrence plots based method for detecting series arc faults in photovoltaic systems," *IEEE Trans. Ind. Electron.*, vol. 69, no. 6, pp. 6308–6315, Jun. 2022.
[31] Q. Yu, G. Huang, and Y. Yang, "Low voltage AC series arc fault detection method based on parallel deep convolutional neural network," *IOP Conf. Ser., Mater. Sci. Eng.*, vol. 490, no. 7, Apr. 2019, Art. no. 072020.
[32] W. Li, Y. Liu, Y. Li, and F. Guo, "Series arc fault diagnosis and line selection method based on recurrent neural network," *IEEE Access*, vol. 8, pp. 177815–177822, 2020.
[33] Y. Wang, L. Hou, K. C. Paul, Y. Ban, C. Chen, and T. Zhao, "ArcNet: Series AC arc fault detection based on raw current and convolutional neural network," *IEEE Trans. Ind. Informat.*, vol. 18, no. 1, pp. 77–86, Jan. 2022.
[34] R. Chu, P. Schweitzer, and R. Zhang, "Series AC arc fault detection method based on high-frequency coupling sensor and convolution neural network," *Sensors*, vol. 20, no. 17, p. 4910, Aug. 2020.
[35] K. Yang, R. Chu, R. Zhang, J. Xiao, and R. Tu, "A novel methodology for series arc fault detection by temporal domain visualization and convolutional neural network," *Sensors*, vol. 20, no. 1, p. 162, Dec. 2019.
[36] R. Chu, R. Zhang, Q. Huang, and K. Yang, "TDV-LSTM: A new methodology for series arc fault detection in low power AC systems," in *Proc. IEEE Sustain. Power Energy Conf. (iSPEC)*, Chengdu, China, Nov. 2020, pp. 2319–2324.
[37] Z. Zhi, L. Liu, D. Liu, and C. Hu, "Fault detection of the harmonic reducer based on CNN-LSTM with a novel denoising algorithm," *IEEE Sensors J.*, vol. 22, no. 3, pp. 2572–2581, Feb. 2022.
[38] *UL Standard for Safety Arc-Fault Circuit-Interrupters*, Underwriters Laboratories, Standard UL1699, May 2017. [Online]. Available: https://standards.globalspec.com
[39] *ARC Fault Circuit Breaker (AFCB), Aircraft, Trip-Free Single Phase and Three Phase 115 VAC, 400 Hz—Constant Frequency*, Standard AS5692A, SAE International, Dec. 2009. [Online]. Available: https://www.sae.org

XIAOLIN LIU was born in Harbin, Heilongjiang, China, in 1978. She received the M.S. degree in detection technology and automation device and the Ph.D. degree in control science and engineering from Yanshan University, China, in 2003 and 2013, respectively. She has been engaged in aircraft cable fault diagnosis for many years. She is currently supervising ten master's students with the Civil Aviation University of China to conduct intelligent fault diagnosis study.

DESHUN HUANG was born in Zunyi, China, in 1997. He received the B.S. degree in electrical engineering and its automation from Soochow University, Jiangsu, China, in 2020. He is currently pursuing the master's degree with the Civil Aviation University of China. His current research interests include aviation cable AC arc fault detection and its application in SSPC.

TAO JING was born in Xi'an, China, in 1982. He received the M.S. degree in power electronics and power transmission from Northwestern Polytechnical University, Xi'an. Currently, he holds a teaching position at the Civil Aviation University of China. He is now engaged in the research and development of aviation EWIS fault diagnosis technology and diagnostic equipment, developing aircraft cable fault diagnosis systems, aircraft cable shield grounding reliability testing systems, multi-load aircraft secondary power distribution SSPC related systems, and achieving certain research results.

YANAN ZHANG was born in Hebei, China, in 1986. She received the M.S. degree in control theory and control engineering from Northeastern University, Shenyang, China, in 2012. She is currently working as a Senior Engineer at AVIC Tianjin Aviation Mechanical & Electrical Company Ltd. Her current research interests include the research and design of aviation secondary power distribution systems.